*Electronic Supplementary Information

Comprehensive morphological and structural investigation of cellulose I and II nanocrystals prepared by sulphuric acid hydrolysis

Wilson Pires Flauzino Neto,[a,b,c,d] Jean-Luc Putaux,[e,f] Marcos Mariano,[c,d] Yu Ogawa,[e,f] Harumi Otaguro,[a] Daniel Pasquini[a] and Alain Dufresne[c,d]

[a] Instituto de Química, Universidade Federal de Uberlândia, Campus Santa Mônica, Av. João Naves de Ávila, 2121, 38400-902, Uberlândia - Minas Gerais, Brazil.

[b] CAPES Foundation, Ministry of Education of Brazil, Brasília - DF 70040-020, Brazil.

[c] Univ. Grenoble Alpes, LGP2, F-38000 Grenoble, France.

[d] CNRS, LGP2, F-38000 Grenoble, France.

[e] Univ. Grenoble Alpes, CERMAV, F-38000 Grenoble, France.

[f] CNRS, CERMAV, F-38000 Grenoble, France.

Birefringence analysis. Vials containing aliquots of 0.15 wt% CNC suspensions were photographed while being placed between crossed polarizers and agitated using a magnetic stirrer.

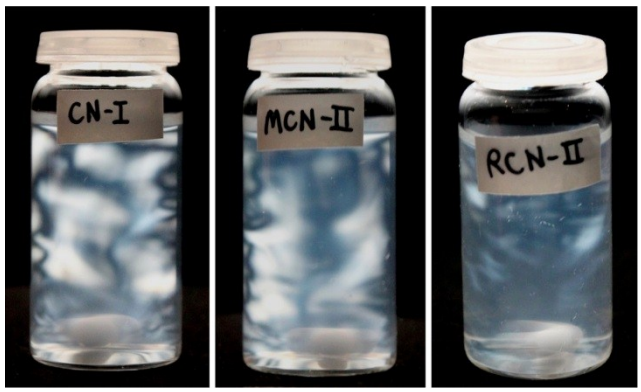

Figure S1. Shear-induced birefringence for 0.15 wt% aqueous suspensions of cellulose nanocrystals under stirring, visualized between crossed polars.

Atomic force microscopy (AFM). AFM measurements of the CNC thickness were performed on a Shimadzu SPM-9600 instrument. Drops of c.a. 0.005 wt% aqueous nanocrystal suspension were left to dry on freshly cleaved mica substrates. 512 × 512-pixel images were recorded at room conditions in the non-contact mode with a scan rate of 1 Hz using Si tips with a curvature radius of less than 10 nm, a spring constant of 42 $N.m^{-1}$ and a resonance frequency of 300 kHz. The images were processed using the VectorScan software. For each sample, about 100 nanoparticles were randomly selected to determine their average thickness.

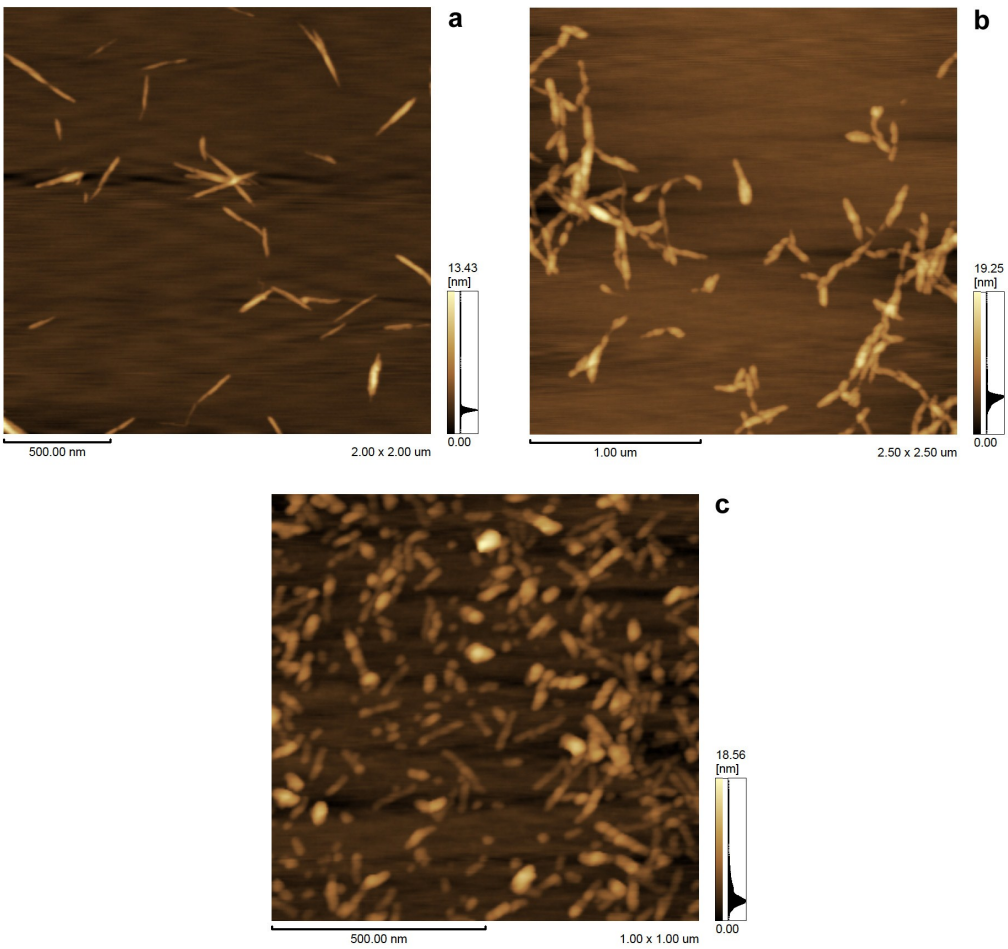

Figure S2. Tapping mode AFM images of CN-I (a), MCN-II (b) and RCN-II (c) nanoparticles.

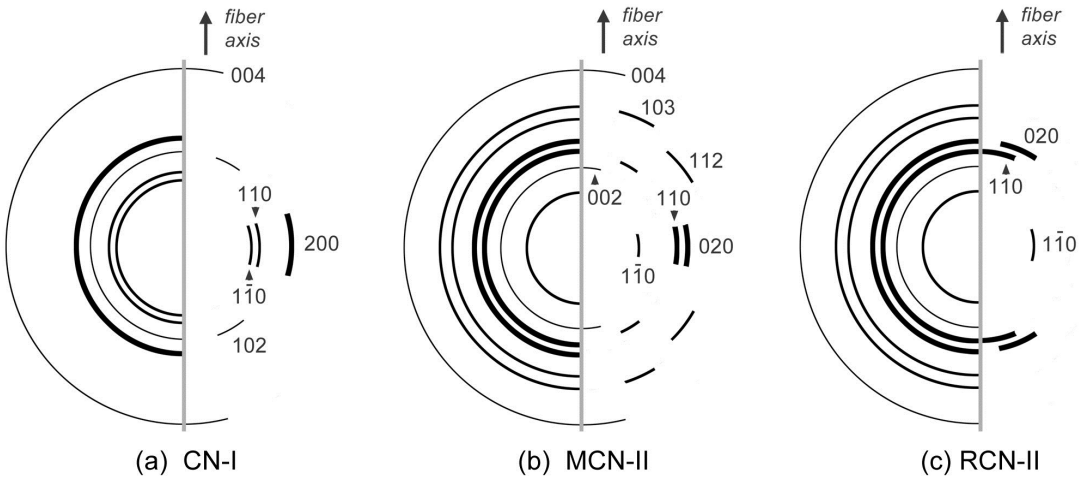

Figure S3. Schematized XRD patterns of the three CNC samples. The left and right halves are powder and fiber patterns, respectively. The fiber axis is vertical. The indices of cellulose Iβ (CN-I) and cellulose II (MCN-II and RCN-II) of the main reflections are indicated.

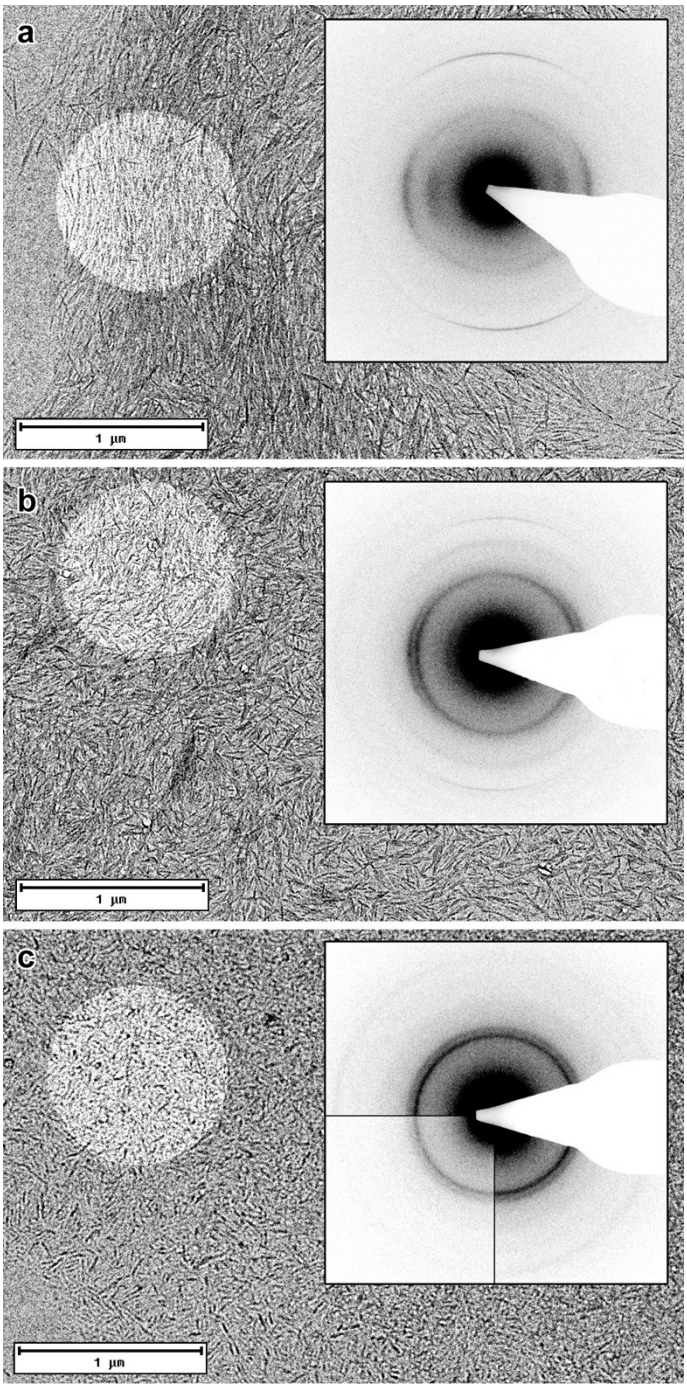

Figure S4. TEM images of unstained preparations for CN-I (a), MCN-II (b) and RCN-II (c) nanoparticles. Insets: corresponding selected area electron diffraction patterns recorded at low temperature. The position of the selected area aperture is indicated in the image. In c, the lower left quarter of the electron diffraction pattern was recorded with a shorter exposure time in order to show that the 110_{II} reflection, closer to the transmitted beam, was absent

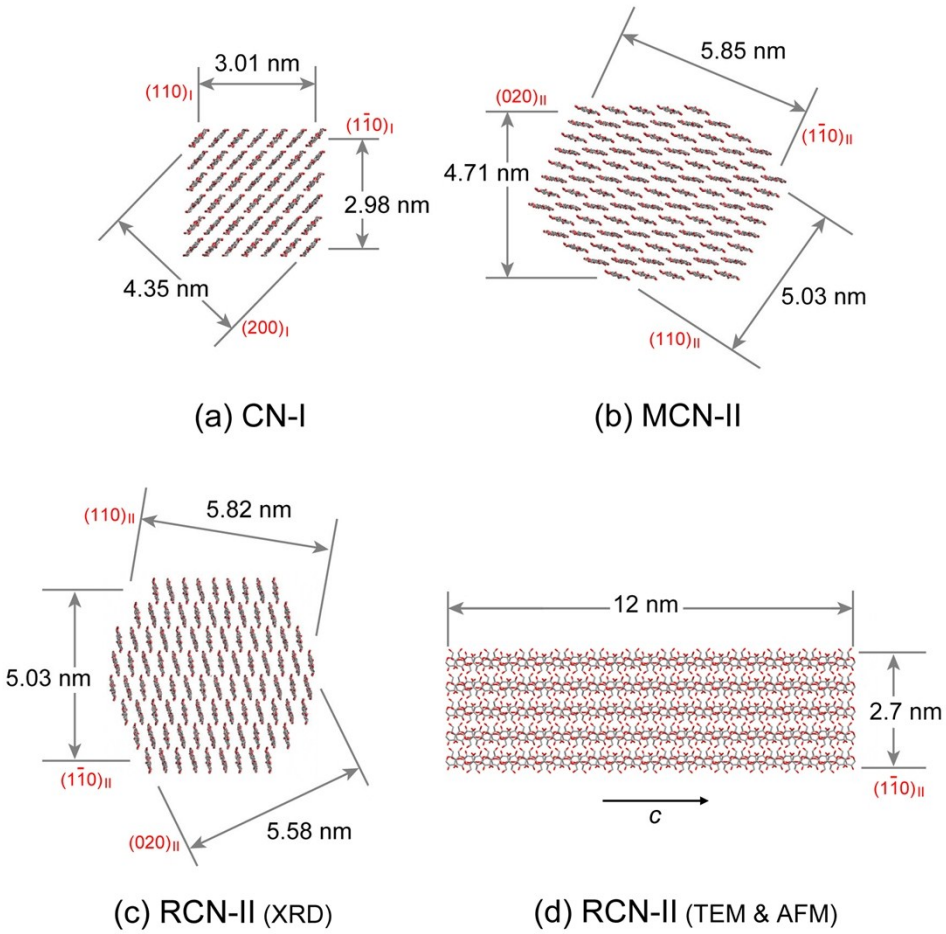

Figure S5. Tentative models of the cross-sections of the elementary crystallites of CN-I (a), MCN-II (b) and RCN-II (c,d) CNCs. In a, b and c, the dimensions have been deduced from the analysis of the peak broadening in the XRD profiles of films. The cellulose chains are viewed along the *c*-axis the crystal lattice of cellulose I (a) and II (b,c). The dimensions D_{hkl} and indices are the values listed in Table 4, not those that would correspond to an integer numbers of crystallographic planes. In d, the dimensions are those estimated from TEM and AFM images of the ribbon-like particles. Note that the model deduced from XRD data of RCN-II crystallites is twice as thick as the one that was estimated from TEM and AFM images. The reason for this discrepancy is not known yet.